Coupling Nanobuilding Block and Breath Figures Approaches for the Designed Construction of Hierarchically Templated Porous Materials and Membranes†

Yoshiaki Sakatani,‡,§ Cédric Boissière,‡ David Grosso,‡ Lionel Nicole,‡ Galo J. A. A. Soler-Illia,⊥ and Clément Sanchez*,‡

Laboratoire de Chimie de la Matière Condensée, Unite Mixte de Recherche, Universite Pierre and Marie Curie−Centre National de la Recherche Scientifique 7574, 4 place Jussieu, 75252 Paris 05, France, Basic Chemicals Research Laboratory, Sumitomo Chemical Co., Ltd., 5-1, Sobiraki-cho, Niihama, Ehime 792–8521, Japan, Unidad de Actividad Quimica, Av. Gral Paz 1499 (1650) San Martín, Buenos Aires, Argentina

Received July 24, 2007. Revised Manuscript Received October 19, 2007

The chemical strategies offered by the coupling of functional nanobuilding blocks (NBBs, made of surface hybrided nanoparticles of SiO_2, TiO_2, Co, and CdS) and breath figures processing allows for the development of new porous materials with hierarchical porosity. Honeycomb-like macroporous membranes or films made of metallic oxides, metals, or chalcogenides having mesoporous walls can be easily obtained. The presented strategy is general, simple, and versatile and allows for the assembling of a large variety of structurally well-defined nanoparticles with very different chemical compositions into complex porous architectures. Moreover, the adjustable size of the nanobuilding block unit permits an easy tuning of the average size of the mesoporosity between 2 and 50 nm.

Introduction

The construction of materials presenting complex hierarchical structures such as those observed in natural materials[1] is a particularly interesting challenge for materials chemists, for it will allow the development of innovative advanced materials with promising applications:[2] chromatography, membranes and smart coatings, catalysis, photovoltaic and fuell cells, sensors, and biosensors. In general, three main approaches are envisaged, based on (i) introducing macrotemplates (size ranging from 100 nm to several micrometers: micropatterned polydimethylsiloxane surfaces,[3] latex or silica nanoparticles,[4–8] large polymers,[9] bacteria,[8,10] etc.) directly into the reaction media, (ii) combining these macrotemplates with usual mesoscale templates (surfactants, molecular agents, etc.),[11] or (iii) by associating phase-separation phenomena and mesoscale-templated cooperative self-assembly.[7,12–16] In particular, materials presenting multiscale porosity present a major interest in catalysis, membranes, and separation-based processes, where optimization of the diffusion and confinement regimes is required. While micro- and mesopores provide the size and shape selectivity for the guest molecules, enhancing the host−guest interactions, the presence of macroporous channels should permit an improvement in access to the active sites on the immediate smaller scale, avoiding pore blocking by reagents or products.[17]

Among the diversity of templating strategies available, the use of "breath figures" (BFs, the fog created by exhaling on a cold surface) as a method to generate texture on the micrometer scale has gained interest.[18] Honeycomb-like macroporous coatings have been prepared by casting in volatile solvents: polymers,[18–26] organic/inorganic hybrid

† Part of the "Templated Materials Special Issue".

* Corresponding author e-mail: clems@ccr.jussieu.fr.
‡ Universite Pierre and Marie Curie−Centre National de la Recherche Scientifique.
§ Sumitomo Chemical Co.
⊥ Unidad de Actividad Quimica.

(1) Sanchez, C.; Arribart, H.; Giraud Guille, M. M. *Nat. Mater.* **2005**, *4*, 277.
(2) Sanchez, C.; Boissiere, C.; Grosso, D.; Laberty, C.; Nicole, L. *Chem. Mat.* **2008**, in press.
(3) Trau, M.; Yao, N.; Kim, E.; Xia, Y.; Whitesides, G. M.; Aksay, I. A. *Nature* **1997**, *390*, 674.
(4) Huang, L. M.; Wang, Z. B.; Sun, J. Y.; Miao, L.; Li, Q. Z.; Yan, Y. S.; Zhao, D. Y. *J. Am. Chem. Soc.* **2000**, *122*, 3530.
(5) Ogasawara, W.; Shenton, W.; Davis, S. A.; Mann, S. *Chem. Mater.* **2000**, *12*, 2835.
(6) Velev, O. D.; Jede, T. A.; Lobo, R. F.; Lenhoff, A. M. *Nature* **1997**, *389*, 447.
(7) Holland, B. T.; Blanford, C. F.; Stein, A. *Science* **1998**, *281*, 538.
(8) Mann, S.; Burkett, S. L.; Davis, S. A.; Fowler, C. E.; Mendelson, N. H.; Sims, S. D.; Walsh, D.; Whilton, N. T. *Chem. Mater.* **1997**, *9*, 2300.
(9) Kramer, E.; Forster, S.; Goltner, C.; Antonietti, M. *Langmuir* **1998**, *14*, 2027.
(10) Davis, S. A.; Burkett, S. L.; Mendelson, N. H.; Mann, S. *Nature* **1997**, *385*, 420.
(11) Yang, P. D.; Deng, T.; Zhao, D. Y.; Feng, P. Y.; Pine, D.; Chmelka, B. F.; Whitesides, G. M.; Stucky, G. D. *Science* **1998**, *282*, 2244.
(12) Soler-Illia, G. J. A. A.; Sanchez, C.; Lebeau, B.; Patarin, J. *Chem. Rev.* **2002**, *102*, 4093.
(13) Wijnhoven, J.; Vos, W. L. *Science* **1998**, *281*, 802.
(14) Jiang, P.; Bertone, J. F.; Colvin, V. L. *Science* **2001**, *291*, 453.
(15) Imhof, A.; Pine, D. J. *Nature* **1997**, *389*, 948.
(16) Tetreault, N.; Miguez, H.; Ozin, G. A. *Adv. Mater.* **2004**, *16*, 1471.
(17) Bunz, U. H. F. *Adv. Mater.* **2006**, *18*, 973.
(18) Widawski, G.; Rawiso, M.; Francois, B. *Nature* **1994**, *369*, 387.
(19) Francois, B.; Pitois, O.; Francois, J. *Adv. Mater.* **1995**, *7*, 1041.
(20) de Boer, B.; Stalmach, U.; Nijland, H.; Hadziioannou, G. *Adv. Mater.* **2000**, *12*, 1581.
(21) Bolognesi, A.; Mercogliano, C.; Yunus, S.; Civardi, M.; Comoretto, D.; Turturro, A. *Langmuir* **2005**, *21*, 3480.

10.1021/cm701986b CCC: $40.75
Published on Web 12/05/2007

polymers,[27] or metallic particles[28–32] are patterned on the micrometer scale under high humidity conditions. BFs are obtained by using, in the presence of moist air, a solution of organic polymers (or as in our case a solution of functional hybrid nanobuilding blocks, NBBs) in an organic volatile solvent ($CHCl_3$, THF, etc.). Evaporation of the solvent leads to a decrease in the air−liquid interfacial temperature of the cast liquid. This evaporative cooling of the solvent induces the condensation of micrometer-sized water droplets on its surface. The condensed water droplets are transferred into the cast liquid by convection of the solvent and assemble in ordered arrays on the liquid surface. After evaporation of the solvent and the water droplets, which act as a template, a honeycomb-like patterned film can be obtained. On the other hand, suitable NBBs with a tailored inorganic core and surface functionality self-assemble in mesoporous structures, introducing the possibility of designing multiscale materials. The use of NBBs presents many advantages:[33] (i) a better definition of the inorganic component with tailored structure and size-dependent properties; (ii) lower reactivity towards chemicals than molecular agents; (iii) an already condensed state allowing for the minimization of sintering and, hence, control of textural porosity; (iv) nanometric, monodisperse, and nanocrystalline NBB components, which facilitates the characterization of the final materials; and (v) a variety found in the NBB nature, structure, and functionality, allowing one to build an amazing range of different architectures and organic−inorganic interfaces. The combination of NBBs with other approaches results in multiscale porous materials. For example, the combined use of BF-driven phase separation and ceria NBBs with defined size and functionality permits the production of polymodal porous CeO_2.[34] If such hierarchically structured porous materials could be obtained without a fancy organic template and from a variety of commercial NBBs, a beneficial process would be achieved in view of a low cost. Previous works have aimed at this problem, providing methods to prepare macroporous thin films composed of hydrophobically functionalized NBBs.[30]

In this work, we present a general strategy which combines the BF templating methods with the NBB approach. To the best of our knowledge, this is the first report of honeycomb-like macroporous films with mesoporous walls induced by the BF method using a large palette of NBBs without polymeric templates. The proposed strategy is general, simple, and versatile and allows direction of the assembling of a large variety of structurally well-defined nanoparticles with very different chemical compositions (silica, transition metal oxides, metals, chalcogenides and probably zeolites, carbides, nitrides, inorganic−organic (or bio-) hybrided nanoparticles, . . .) into complex porous architectures. Moreover, the adjustable size of the nanobuilding unit permits an easy tuning of the mean size of the mesoporosity between 2 and 50 nm.

Experimental Section

Premade functional NBBs were used as hybrid inorganic−organic precursors to produce multiscale porous films or xerogels. The NBBs were either synthesized by previously reported techniques or were obtained upon modification of commercially available products.

Surfactants. $C_nH_{2n+1}NH_4Br$ (n = 6–16), $C_nH_{2n+1}COOH$ (n = 3–13) (b), $C_nH_{2n+1}COOH$ (n = 5–13), and $C_nH_{2n+1}SH$ (n = 6–14) were used as surfactants. Among them, $C_{12}H_{25}NH_4Br$, $C_{11}H_{23}COOH$, $C_9H_{19}COOH$, and $C_{10}H_{21}SH$ were referred to as DDTM, LA, DA, and DT, respectively.

SiO_2 and TiO_2 Particles. Fumed SiO_2 (Sigma-Aldrich, 99.8%, 0.014 μm) and TiO_2 (Alfa, 99.9 %, anatase) were used as NBBs. A 30 nm crystallite size was found for TiO_2 by X-ray diffraction (XRD; Debye-Scherrer formula, anatase (101) peak).

Co Metal Particles. Surfactant-modified Co particles were prepared by a method adapted from Pileni and coworkers.[35] Bis(2ethylhexyl)sulfosuccinate (AOT)/Co^{2+} reverse micelles (molar ratio: AOT/Co = 2, 0.1 M) were prepared by adding an AOT/isooctane solution (0.23 M) to a $CoCl_2$ aqueous solution (molar ratio: H_2O/AOT = 40, 0.75 M). Subsequently, a $NaBH_4$ aqueous solution (0.1 M) was added to the AOT/Co^{2+} micelle dispersion (molar ratio: $NaBH_4$/Co = 3), followed by addition of the surfactant dissolved in an isooctane solution (1.0 M; molar ratio: surfactant/Co = 2), and washing of the AOT and excess surfactant with ethanol. The obtained solid was dried in a N_2 environment at room temperature and then was redispersed in chloroform. Heated DA/Co particles were prepared by heating DA/Co particles dispersed in isooctane with DA (the same amount of DA used in the preparation of DA/Co particles) at 110 °C for 3 h, followed by washing of the excess DA with ethanol. The obtained solid was dried in a N_2 environment at room temperature and then was redispersed in chloroform.

CdS Particles. Surfactant-modified CdS particles were prepared by a method adapted from Harruff and Bunker.[36] An AOT/Cd^{2+} micellar dispersion was prepared by adding AOT dissolved in isooctane (0.5 M) to a $Cd(CH_3COO)_2$ aqueous solution (0.5 M; molar ratio: AOT/Cd^{2+} = 15, H_2O/AOT = 7). An AOT/S^{2-} dispersion was obtained in a similar way, using a Na_2S aqueous solution (0.5 M; molar ratio: AOT/S^{2-} = 7, H_2O/AOT = 15). A color change was observed upon the addition of AOT/S^{2-} to AOT/Cd^{2+} (molar ratio: Cd^{2+}/S^{2-} = 1). After 10 min of this addition, alkylthiol was added to the AOT/CdS chloroform solution (molar ratio: surfactant/AOT = 1), followed by washing of the excess AOT and surfactants with ethanol. The obtained solid was dried in a N_2 environment at room temperature and then was redispersed in chloroform.

(22) Peng, J.; Han, Y. C.; Yang, Y. M.; Li, B. Y. *Polymer* **2004**, *45*, 447.
(23) Nishikawa, T.; Nishida, J.; Ookura, R.; Nishimura, S. I.; Wada, S.; Karino, T.; Shimomura, M. *Mater. Sci. Eng., C* **1999**, *10*, 141.
(24) Maruyama, N.; Koito, T.; Nishida, J.; Sawadaishi, T.; Cieren, X.; Ijiro, K.; Karthaus, O.; Shimomura, M. *Thin Solid Films* **1998**, *329*, 854.
(25) Xu, Y.; Zhu, B.; Xu, Y. *Polymer* **2005**, *46*, 713.
(26) Zhao, B. H.; Zhang, J.; Wang, X. D.; Li, C. X. *J. Mater. Chem.* **2006**, *16*, 509.
(27) Karthaus, O.; Cieren, X.; Maruyama, N.; Shimomura, M. *Mater. Sci. Eng. C* **1999**, *10*, 103.
(28) Yonezawa, T.; Onoue, S.; Kimizuka, N. *Adv. Mater.* **2001**, *13*, 140.
(29) Maillard, M.; Motte, L.; Ngo, A. T.; Pileni, M. P. *J. Phys. Chem. B* **2000**, *104*, 11871.
(30) Shah, P. S.; Sigman, M. B.; Stowell, C. A.; Lim, K. T.; Johnston, K. P.; Korgel, B. A. *Adv. Mater.* **2003**, *15*, 971.
(31) Saunders, A. E.; Shah, P. S.; Sigman, M. B.; Hanrath, T.; Hwang, H. S.; Lim, K. T.; Johnston, K. P.; Korgel, B. A. *Nano Lett.* **2004**, *4*, 1943.
(32) Li, J.; Peng, J.; Huang, W. H.; Wu, Y.; Fu, J.; Cong, Y.; Xue, L. J.; Han, Y. C. *Langmuir* **2005**, *21*, 2017.
(33) Sanchez, C.; Soler-Illia, G. J. A. A.; Ribot, F.; Lalot, T.; Mayer, C. R.; Cabuil, V. *Chem. Mater.* **2001**, *13*, 3061.
(34) Bouchara, A.; Mosser, G.; Siker-Illia, G.; Chane-Ching, J. Y.; Sanchez, C. *J. Mater. Chem.* **2004**, *14*, 2347.
(35) Petit, C.; Wang, Z. L.; Pileni, M. P. *J. Phys. Chem. B* **2005**, *109*, 15309.
(36) Harruff, B. A.; Bunker, C. E. *Langmuir* **2003**, *19*, 893.

Preparation of the Porous Cast Xerogels or Films. SiO_2- and TiO_2-containing casting dispersions were obtained by adding these nanopowders to surfactant-containing chloroform (for SiO_2) or THF (for TiO_2) solutions, under stirring at room temperature. The surfactant adsorbed onto these nanopowders and allowed them to be dispersed in the solution.

For Co and CdS casting dispersions, the surfactant-modified Co and CdS particles were directly dispersed in chloroform. The films were prepared by casting the dispersions on a clean glass slide in a controlled humidity chamber at room temperature (15–20 °C). The concentration in the cast dispersions and the cast volumes were 0.1 wt % and 30 μL for SiO_2, 3.0 wt % and 15 μL for TiO_2, and 1.0 wt % and 30 μL for Co and CdS, respectively. In order to remove the surfactant from SiO_2- and TiO_2-based films, the films were calcined at 300 °C for 1 h, then at 400 °C for 20 min, and finally at 500 °C for 15 min in the air.

Characterization. XRD patterns of the obtained film were collected on a Bruker D8 apparatus and a PW 1830 Philips ($\lambda_{CuK\alpha}$) apparatus. The porous morphologies of the obtained films were observed by scanning electron microscopy (SEM) with a Cambridge Treroscan 120 apparatus. Thermogravimetric (TG) analysis was carried out on SDT 2960-TA apparatus. N_2 adsorption−desorption isotherms and the Brunauer−Emmett−Teller (BET) surface area were measured using a Micromeritics ASAP 2010 physisorption analyzer. UV−visible spectra were measured using a Bio-Tek Instruments UVIKON XS spectrophotometer. The average dispersed particle size was measured using Brookhaven Instruments Zeta plus equipment.

Photocatalytic Reaction of LA/TiO_2. Prior to the reaction, the 500 °C calcined LA/TiO_2 film was irradiated with UV light (24 W-λ = 365 nm) overnight to decompose pollutants adsorbed on its surface. Then, the calcined LA/TiO_2 film was placed in a Petri dish filled with a 10 μM methylene blue (MB) aqueous solution (10 mL) and was allowed to adsorb MB in the dark overnight. An absorbance of MB solution corresponding λ = 665 nm was measured by UV−visible spectroscopy versus irradiation time. The amount of MB decomposition was determined by a linear relationship between the concentration and the absorbance of MB.

Results and Discussion

The mechanism of BF templating is illustrated in Figure 1. A macroporous structure is obtained from the controlled condensation of water droplets on the solid surface of a film, which is formed upon volatile solvent evaporation. The temperature decrease due to the evaporation of the volatile solvent locally reduces the temperature below the water dew point; water condensation is thus induced. The water microdroplets formed penetrate the film upon formation, creating an organized pore pattern on the micrometer−submicrometer scale. The film in formation has to be maleable enough to permit generation of the pores. Typically, polymers are well-suited to this purpose; recent work has shown that functional nanoparticles can be used in combination with polymers, to obtain macroporous arrays.[17,30,37] Our strategy relies in the use of an array of organically modified NBB as a flexible matrix that can adapt to the changes brought by water condensation on the film surface. In this framework, several aspects are extremely important: the solvent evaporation rate, the rate of the water condensation process, the hydrophilic−hydrophobic character of the NBB, the role of added surfactants, the NBB size or sinterability, and so forth. In the following, we will analyze these aspects for a variety of modified NBB systems.

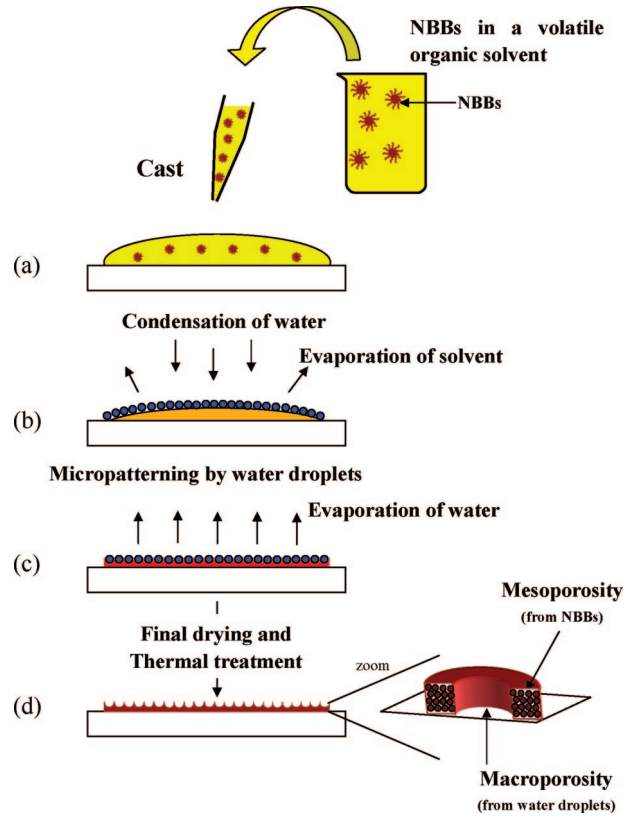

Figure 1. Illustration of the mechanism of BF. (a) Cast of NBBs' solution on a substrate, (b) formation of water microdroplets, (c) close packing of water microdroplets, and (d) formation of pore pattern on the micronic−submicronic scale.

Influence of the Environmental Humidity upon the Porous Morphology. Previous work reported that the formation of the porous morphology depends upon an environmental relative humidity (RH).[22,24,26,31] High RH is required to form surface water droplet arrays upon solvent evaporation. The formation of macropores in high humidity atmospheres is strong proof that the BF templating path is being followed. Spinodal phase separation, instead, takes place in a narrow optimal RH range, where the interactions between the inorganic oligomers, an organic polymer, and the evaporating solvent lead to complex behavior.[38–40] We conducted a systematic investigation in a number of systems, representative of metals, semiconductors, or oxides. The behavior pattern found towards RH was similar in all examined systems. Figure 2 shows that the porous morphologies were observed in DDTM/SiO_2, LA/TiO_2, and DT/CdS films when the environmental humidity was at more than 80% RH. Moreover, macroporous patterns were observed in metallic DA/Co films when prepared at more than 70%

(37) Boker, A.; Lin, Y.; Chiapperini, K.; Horowitz, R.; Thompson, M.; Carreon, V.; Xu, T.; Abetz, C.; Skaff, H.; Dinsmore, A. D.; Emrick, T.; Russell, T. P. *Nat. Mater.* **2004**, *3*, 302.
(38) Nakanishi, K. *J. Porous Mater.* **1997**, *4*, 67.
(39) Kajihara, K.; Nakanishi, K.; Tanaka, K.; Hirao, K.; Soga, N. *J. Am. Ceram. Soc.* **1998**, *81*, 2670.
(40) Fuertes, M. C.; Soler-Illia, G. J. A. A. *Chem. Mater.* **2006**, *18*, 2109.

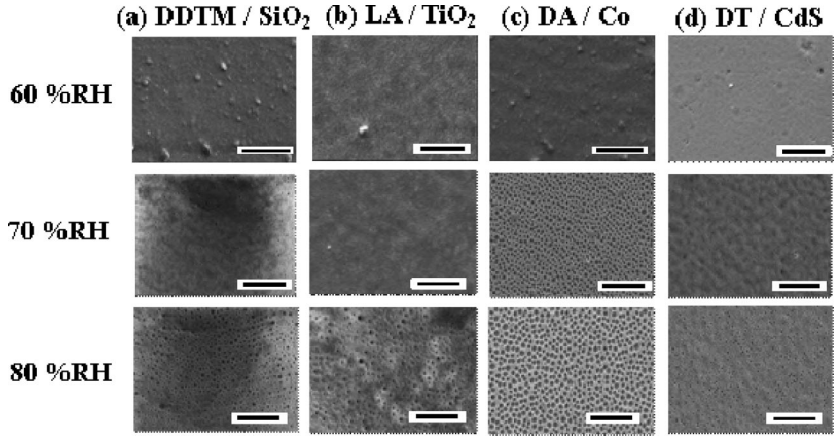

Figure 2. SEM images of (a) DDTM/SiO_2, (b) LA/TiO_2, (c) DA/Co, and (d) DT/CdS films fabricated by casting under 60–80% RH at room temperature. The molar ratios of DDTM to SiO_2 and LA to TiO_2 were fixed at 0.4. Scale bar: 50-μm-long.

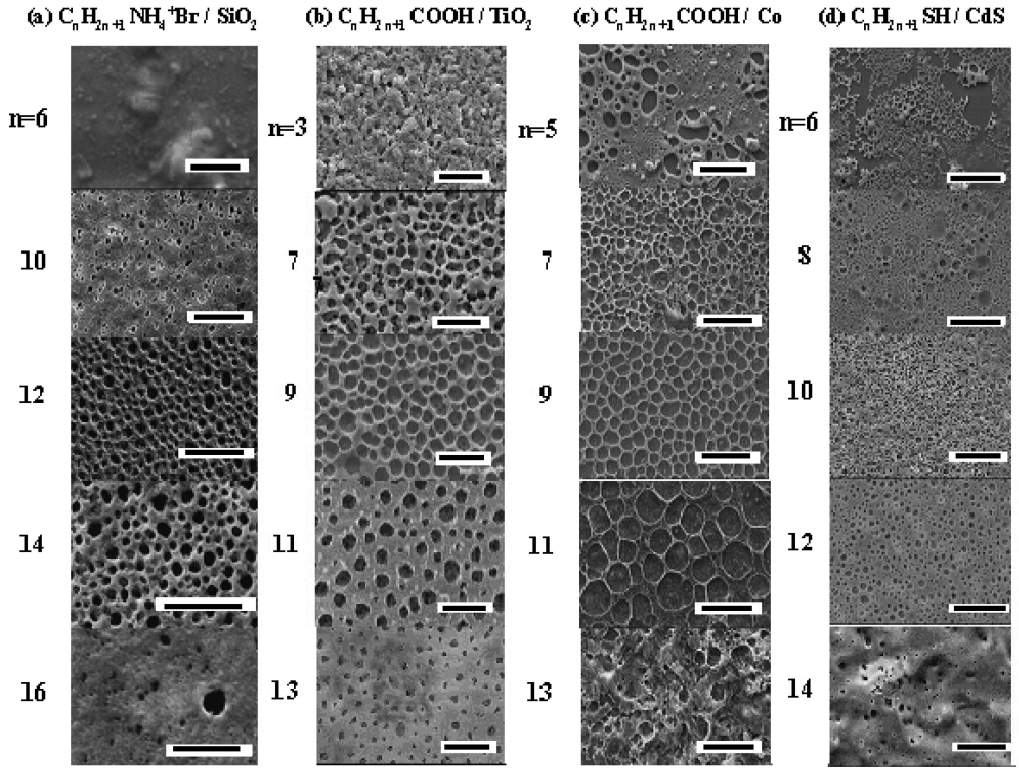

Figure 3. SEM images of $C_nH_{2n+1}NH_4Br/SiO_2$ (n = 6–16) (a), $C_nH_{2n+1}COOH/TiO_2$ (n = 3–13) (b), $C_nH_{2n+1}COOH/Co$ (n = 5–13) (c), and $C_nH_{2n+1}SH/CdS$ (n = 6–14) (d) films that were fabricated by casting under 90% RH at room temperature. The molar ratios of $C_nH_{2n+1}NH_4Br$ to SiO_2 and $C_nH_{2n+1}COOH$ to TiO_2 were fixed at 0.4. Scale: 20-μm-long (a and b) and 50-μm-long (c and d).

RH (Figure 2c). In all films, pore size and pore densities were observed to increase with increasing RH, as previously reported for polymer films under controlled RH conditions.[22] The kinds of surfactants and NBBs influenced the condensation of the water microdroplets on the NBB dispersed solution. DA-modified Co NBBs made it possible to stabilize the water microdroplets under even 70% RH. The porous morphology could not be formed in all films under a controlled ethanol vapor environment. Ethanol did not allow a formation of microdroplet arrays on the films because the surfactants could solve in ethanol and did not stabilize ethanol as the microdroplet. These findings prove that the water droplets condensed on the film surface acted as a template of the macroporous morphology.

Control of Hydrophilic and Hydrophobic Proportion in the Cast Liquid by Addition of Surfactants. In ordered polyion complex-based honeycomb-like porous films prepared by casting under high humidity conditions, the presence of a hydrophilic function, such as polar groups, stabilizes the condensed water droplets, the hydrophobic part preventing their coalescence.[23] The proportion between hydrophilic and hydrophobic fractions is an important factor in the assembly of the water droplets in micrometer-sized arrays, and the co-assembly of the water droplets and the inorganic NBB. A systematic variation of the surface function was

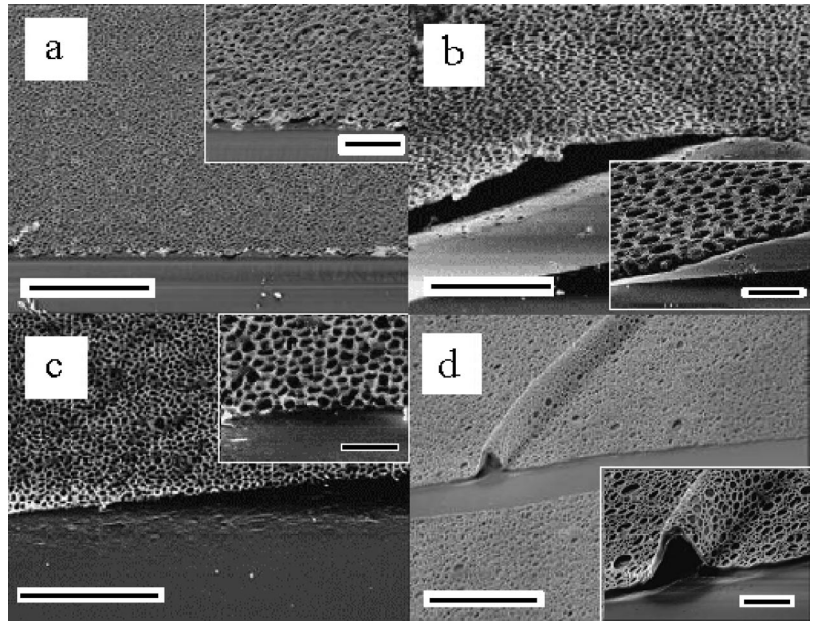

Figure 4. SEM images of DDTM/SiO_2 (a), LA/TiO_2 (b), DA/Co (c), and DT/CdS (d) films that were fabricated by casting under 90% RH at room temperature. The molar ratios of DDTM to SiO_2 and LA to TiO_2 were fixed at 0.4. Scale: 100-μm-long (a, c, and d), 50-μm-long (b), 20-μm-long (inset of a, c, and d) and 10-μm-long (inset of b).

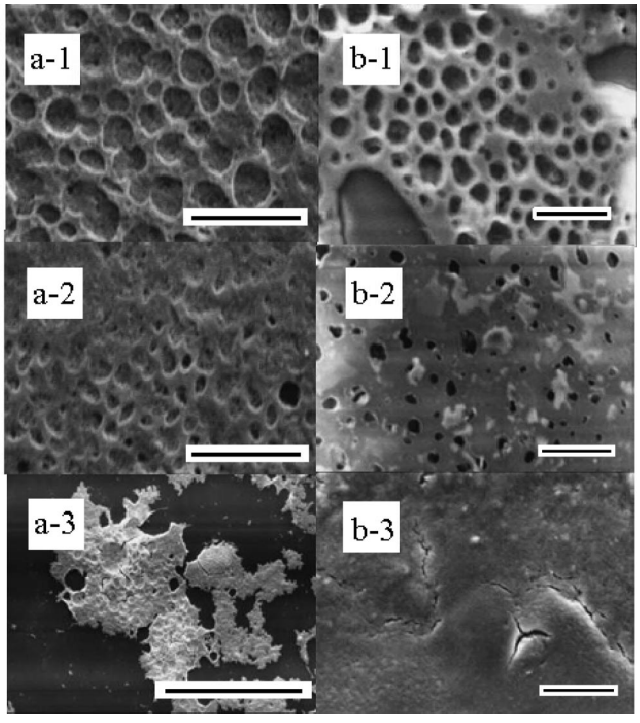

Figure 5. SEM images of (a) DDTM/SiO_2 and (b) LA/TiO_2 films prepared by casting under 90% RH at room temperature. The molar ratios of DDTM to SiO_2 and LA to TiO_2 were 0.2 (a-1 and b-1) and 0.6 (a-2 and b-2). The excess of DDTM and LA were washed off with ethanol and then redispersed in chloroform (for SiO_2) and THF (for TiO_2) (a-3 and b-3). Scale bars are 20-μm-long (except for a-3) and 200-μm-long (a-3).

performed. The NBB surfaces were modified by using surfactants with a variety of polar head groups compatible with the NBB surface: ionic ($C_nH_{2n+1}NH_4Br$) for SiO_2, carboxylate ($C_nH_{2n+1}COOH$) for TiO_2 and Co, and thiol ($C_nH_{2n+1}SH$) for CdS. Figure 3 shows the films prepared by casting liquids under an optimal RH of 90%, at room temperature. The honeycomb-like porous morphologies were observed when n was at 12–14 for $C_nH_{2n+1}NH_4Br/SiO_2$, at

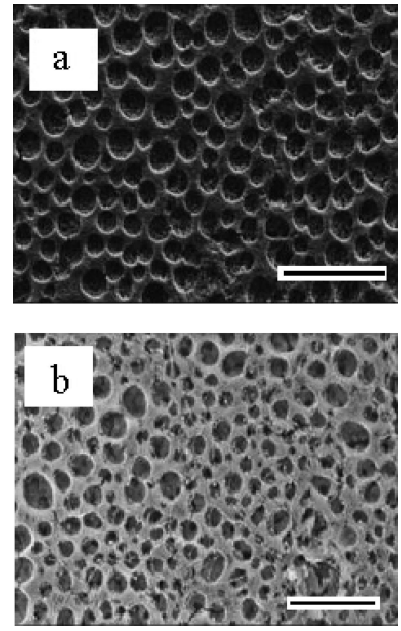

Figure 6. SEM images of the 500 °C calcined DDTM/SiO_2 (a) and LA/TiO_2 (b) films. As-prepared films were obtained by casting under 90% RH at room temperature. The molar ratio of DDTM to SiO_2 and LA to TiO_2 were fixed at 0.4. Scale bars are 20-μm-long.

7–11 for $C_nH_{2n+1}COOH/TiO_2$ and $C_nH_{2n+1}COOH$/Co, and at 10–12 for $C_nH_{2n+1}SH$/CdS. A shorter surfactant carbon chain imparts stronger hydrophilic properties to the cast liquid, leading to a coalescence of the water droplets. On the other hand, the surfactants having a larger carbon chain increase the hydrophobic property of the NBB suspended in the cast liquid, deteriorating the stability of the condensed water droplets. The surfactants described above achieved the optimal hydrophilic and hydrophobic proportions in each of the cast liquids to fabricate the honeycomb-like porous films.

The molar ratio of $C_nH_{2n+1}NH_4Br$ to SiO_2 and $C_nH_{2n+1}COOH$ to TiO_2 in the cast liquid was fixed at s =

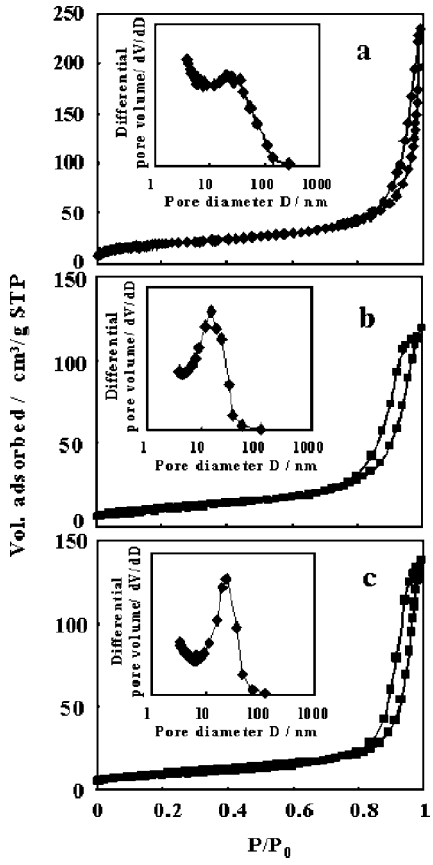

Figure 7. N_2 adsorption−desorption isotherms of the 500 °C calcined (a) DDTM/SiO_2, (b) LA/TiO_2, and (c) LA/TiO_2 (25% RH) powders. As-prepared samples were obtained by casting under 90% RH (a and b) and 25% RH (c) at room temperature. The molar ratios of DDTM to SiO_2 and LA to TiO_2 were fixed at 0.4. Inset: BJH pore size distributions that were calculated from the desorption branch of the isotherms a, b, and c.

0.4. These cast liquids contained an excess of the surfactants. In contrast, $C_nH_{2n+1}COOH$/Co- and $C_nH_{2n+1}SH$/CdS-based honeycomb-like porous films were not obtained when the cast liquids had an excess of the surfactants. Previous work reported that the excess surfactant was removed in the cast liquids when preparing Au- and Ag-based honeycomb-like porous films.[28–32] The different behavior observed between oxides (SiO_2 and TiO_2) and other NBB-based (Co and CdS) films is caused by the hydrophilic property of the cast liquids. Without the surfactant excess, the oxide-based cast liquids exhibited stronger hydrophilic properties than the latter one due to the surface hydrophilic OH groups. The surfactant excess provides the relatively hydrophilic oxide NBB with a hydrophobic character, in order to achieve the optimum hydrophilic and hydrophobic proportion. The influences of the surfactant-to-metal ratio upon pore morphologies are discussed below.

Figure 4 shows SEM images of DDTM/SiO_2 (a), LA/TiO_2 (b), DA/Co (c), and DT/CdS (d) films. All films have a thickness of ca. 3 μm and consist of a single porous layer. A gap was formed between the film and the glass slide substrate in Figure 4b and c, when the film-coated glass slides were cropped in order to measure their cross-section. A few cracks and typical wrinkles were observed in DT/CdS film (Figure 4d), which means that tensile stress was generated after the formation of the porous morphology. Dodecanethiol/CdS-based films showed the same cracks as the DT/CdS one. Porous films shown in Figure 3 did not exhibit peaks in low-angle XRD patterns (not shown), indicating that no ordered mesoporous structure is obtained under these conditions.

Influence of the Molar Ratio of Surfactant to SiO_2 and TiO_2 upon the Porous Morphology. In order to prepare ceramic powder slurries, small amounts of dispersants are usually used. In this study, when the DDTM/SiO_2 and LA/TiO_2 molar ratio (s) was 0.4, the respective weight ratios of DDTM/SiO_2 and LA/TiO_2 were approximately 2 and 1, respectively. DDTM/SiO_2 and LA/TiO_2 films with $0.2 \leq s \leq 0.6$ were prepared in order to assess the influence of the surfactants upon the film morphology. The porous films in which $s = 0.2$ (Figure 5a-1 and b-1) present a larger pore size than those in which $s = 0.4$ (Figure 3a, $n = 12$ and Figure 3b, $n = 11$). The cast liquids with a lower surfactant ratio (DDTM or LA) present a higher solvent vapor pressure than the more concentrated ones,[14] and NBB with a higher hydrophilic character. As a consequence, the temperature gradient is higher for the low surfactant samples, leading to an increase of the condensed water droplet size. The stronger hydrophilic properties of the NBBs remaining after drying, and the larger size of the water droplets, result in larger macropores. The honeycomb-like porous morphologies were not formed for $s > 0.6$ (Figure 5a-2 and b-2). The cast films are relatively hydrophobic, due to the increase in DDTM or LA, and water condensation does not take place, preventing the formation of a macroporous morphology. The excess DDTM and LA were washed off with ethanol, and then the obtained solid could be redispersed in chloroform (for SiO_2) and THF (for TiO_2), followed by casting them at 90% RH at room temperature. The obtained films did not show a macroporous morphology as demonstrated in Figure 5a-3 and b-3, proving that an optimal amount of free DDTM and LA improves the stabilization of the condensed water droplets.

Calcination of SiO_2- and TiO_2-Based Porous Films. Honeycomb-like porous films presenting multiscale porosity are interesting for various applications. The elimination of the organic components was carried out by a gentle thermal treatment in the air. SEM images of 500 °C calcined DDTM/SiO_2 and LA/TiO_2 films are shown in Figure 6a and b, respectively. The honeycomb-like porous morphologies were maintained up to 500 °C, as demonstrated by a comparison of Figure 6 with the as-prepared films (Figure 3a, $n = 12$, and b, $n = 11$). TG measurements for DDTM/SiO_2 and LA/TiO_2 demonstrate that the organic modifiers can be completely removed by pyrolysis up to 300 and 400 °C, respectively, with weight losses of 66.5 wt % for DDTM/SiO_2 and 53.5 wt % for LA/TiO_2 ($s = 0.4$). These values were in good agreement with the respective theoretical values of 67.3 and 50.1 wt % (Supporting Information).

The N_2 adsorption−desorption isotherm of the calcined film on the substrate could not be measured directly, due to the small amount of film. Instead, isotherms were run on samples of the calcined powders obtained by casting 3 mL of the initial suspensions on a large-size Petri dish under the same conditions as DDTM/SiO_2 and LA/TiO_2 honeycomb-

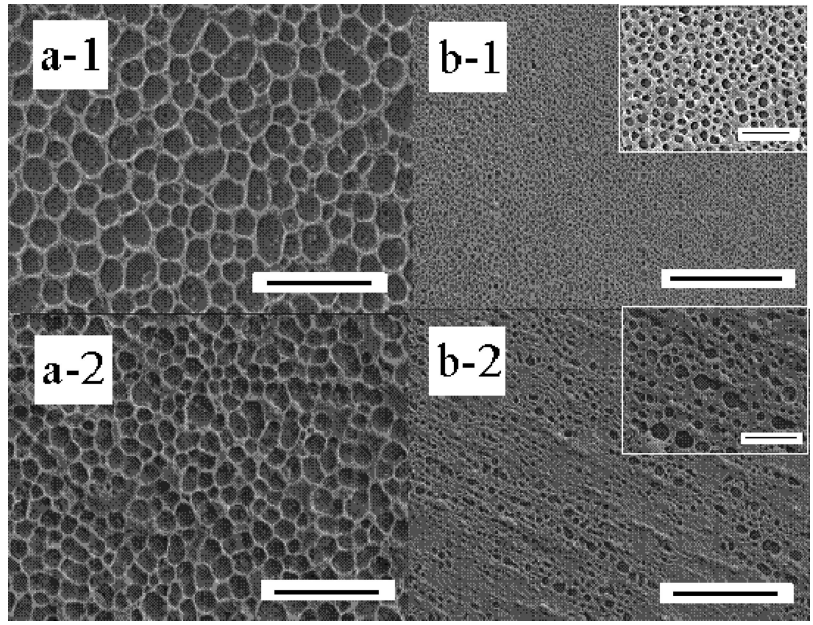

Figure 8. SEM images of BF-templated macroporous films made of (a) as-made DA/Co and (b) DA/Co NBB heated at 110 °C for 3 h. These films were fabricated by casting with a volume of 30 μL of DA/Co and the heated-DA/Co particle (1.0 wt %) dispersed chloroform solution under 90% RH at room temperature. The formation of the a-2 and b-2 films were carried out on a glass slide placed on top of a commercial magnet. Scale: 50-μm-long (a-1, a-2, and insets of b-1 and b-2) and 200-μm-long (b-1 and b-2).

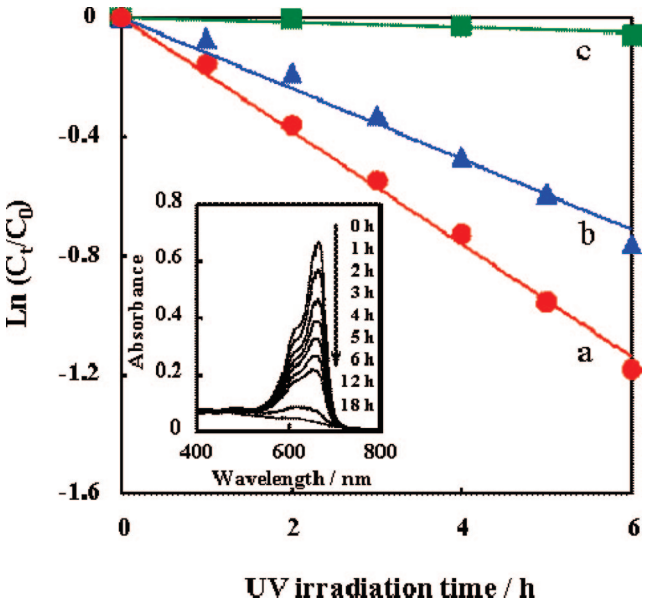

Figure 9. The results of photocatalytic decomposition of methylene blue over the 500 °C calcined (a) macro-mesoporous LA/TiO_2 film, (b) the non-macroporous one, and (c) a control (without photocatalyst) under UV light irradiation. The LA/TiO_2 films were prepared under 90% RH (a) and 25% RH (b) at room temperature with a molar ratio LA to TiO_2 of 0.4. The inset indicates variation of the absorption spectra of methylene blue over the calcined LA/TiO_2 film (a) under UV light irradiation.

like porous films (90% RH, room temperature) followed by peeling and then calcining at 500 °C in the air. The isotherms of the calcined DDTM/SiO_2 and LA/TiO_2 powders are displayed in Figure 7a and b, respectively. Their corresponding Barrett−Joyner−Halenda (BJH) pore size distributions are shown in the Figure 7 insets. The calcined DDTM/SiO_2 powder displayed a broad pore distribution and had a pore volume of 0.30 cm^3/g and BET surface area of 69 m^2/g. On the other hand, the calcined LA/TiO_2 also showed a wide pore distribution and had a pore volume of 0.18 cm^3/g and BET surface area of 39 m^2/g. The isotherms are type IV, and their shapes imply that the calcined DDTM/SiO_2 and LA/TiO_2 are mesoporous. The origin of this mesoporosity is the voids in the interparticle space of aggregated particles.[41] A calcined LA/TiO_2 powder was prepared in a similar way, except that the casting took place under 25% RH, followed by thermal treatment. These preparation conditions did not result in a honeycomb-like porous morphology. The N_2 adsorption−desorption isotherm and the pore size distribution of the calcined LA/TiO_2 (25% RH) are shown in Figure 7c. The resulting calcined powder had a pore volume of 0.20 cm^3/g and BET surface area of 35 m^2/g. These results were similar to those obtained in the macroporous LA/TiO_2 calcined porous powder (Figure 7b). This indicates that the humidity of the cast environment did not influence upon the formation of the mesoporous structure. A similar result was obtained for macro-mesoporous titania thin films produced by controlled-phase separation, where most of the porosity and surface area derive from the mesopores, and macropores account for a minor surface area.[40]

The average dispersed particle size of DDTM/SiO_2 and LA/TiO_2 measured by DLS yields 238 nm (in chloroform) and 460 nm (in THF), respectively, indicating that the initial NBBs are aggregated in the solvent. These aggregated particles assemble as building blocks upon drying and water coalescence, forming DDTM/SiO_2 and LA/TiO_2 honeycomb-like porous film with a disordered mesoporous structure through a *breath figures* templating method.

Influence of the Magnetic Field upon the Formation of DA/Co-Based Porous Film. Nanocrystalline Co particles are one of the most attractive magnetic nanomaterials. Apart from the templating effects observed by using the BF method,

(41) Konishi, J.; Fujita, K.; Nakanishi, K.; Hirao, K. *Chem. Mater.* **2006**, *18*, 864.

the influence of an external magnetic field to macro-mesoporous films made up of magnetic NBBs provides the possibility of yielding a multitemplating effect. An external magnetic field was applied upon the formation of the porous morphology of a DA/Co film using a commercial magnet (size: inner diameter, 25 mm; external diameter, 55 mm; thickness, 8 mm) for the films placed under 90% RH at room temperature. The magnetic influence is negligible for as-prepared Co NBBs, as shown in Figure 8a-1 and a-2. An annealing treatment (110 °C for 3 h) was applied to the Co NBBs; this heat treatment hardly improves the crystallinity of DA/Co particles (see Supporting Information) but seems to promote the NBB aggregation in the suspension, leading to an increase of the average dispersed particle size of DA/Co in chloroform from 177 to 213 nm. This results in an increase of the pore wall thickness due to the aggregation of DA/Co particles. Figure 8b-1 and b-2 show SEM images of the heated DA/Co particle-based film that was prepared on the magnetic field under 90% RH at room temperature. The pores appear arranged along the magnetic field lines. This result indicates that the BF method can be combined with an external solicitation such as a magnetic field, in order to control the pore arrangement of magnetic NBB.

Control of Nanoproperties in LA/TiO_2 BF-Templated Films. The catalytic properties characteristic of the NBB used to create BF-templated multiporous structures are retained in the BF-templated materials, with the additional advantage of a macro-mesoporous structure. We can illustrate this with an example using the well-known titania photocatalysis, studied extensively for application in water and air purification. Herein, the photocatalytic activities of the 500 °C calcined honeycomb-like porous LA/TiO_2 film and a non-macroporous one (synthesized at 25% RH, see above) were evaluated by the decomposition rate of methylene blue (MB) under UV light irradiation. The decomposition reaction of MB could be expressed as a first-order reaction, $\mathrm{Ln}(C_t/C_0) = -kt$ (C_0 and C_t, concentrations of MB at $t = 0$ and $t = t$; k, rate constant). The photon irradiation having higher energy than the band gap of the photocatalyst provides excited electrons in the conduction band and holes in the valence band. The photo-generated electrons and holes react with oxygen and water from the environment to produce active oxygen and radical species, which decompose organic compounds into CO_2 and H_2O. Figure 9 plots the results of the decomposition of MB as the first-order reaction. Rate constants were estimated as 0.19/h for the calcined honeycomb-like porous LA/TiO_2 and 0.12/h for the non-macroporous one. While both films show similar surface areas and pore sizes, the former showed 1.6 times higher activity than the latter. The superior photocatalytic activity of the calcined macro-mesoporous TiO_2 film can be explained on the basis of its hierarchical porosity. The porous morphology made it possible to irradiate UV light to the film inside effectively, and to achieve the generation of a large amount of active oxygen and radical species, resulting in the high photocatalytic activity.[42] The nested macropore−mesopore pore structure seems to help diffusion of the reagents and degradation products in and out the catalyst, therefore enhancing the activity.

Conclusions

We demonstrated that the breath figures method is suitable for the preparation of surfactant-modified SiO_2-, TiO_2-, Co-, and CdS-based honeycomb-like porous films. These films were obtained by a cast method under at least more than 80% RH at room temperature. Condensed water droplets on the cast liquid worked as a template. The hydrophilic and hydrophobic proportion in the cast liquid, which can be controlled by a chain length of surfactants, is indeed an important factor in formation of the condensed water droplet arrays. We found that optimum surfactants were $C_nH_{2n+1}NH_4Br$ (n = 12–14) for SiO_2, $C_nH_{2n+1}COOH$ (n = 7–11) for TiO_2 and Co, and $C_nH_{2n+1}SH$ (n = 10–12) for CdS. The honeycomb-like porous morphologies of $C_{12}H_{25}NH_4Br$/SiO_2- and $C_{11}H_{23}COOH$/TiO_2-based films were maintained through calcinations at 500 °C. The 500 °C calcined TiO_2 porous film exhibited higher photocatalytic activity than the calcined non-porous one. A heat treatment at 110 °C provided $C_9H_{19}COOH$/Co particles with magnetic properties, and an external magnetic field influenced the formation of the $C_9H_{19}COOH$/Co-based honeycomb-like porous film.

Acknowledgment. We thank Sumitomo Chemical Co. Ltd. for scientific and financial support.

Supporting Information Available: Figures illustrating TG analysis of DDTM/SiO_2 and LA/TiO_2, XRD patterns of DA/Co and DT/CdS particles, and UV−vis spectrum of DT/CdS. This material is available free of charge via the Internet at http://pubs.acs.org.

CM701986B

(42) Kato, K.; Tsuzuki, A.; Torii, Y.; Taoda, H.; Kato, T.; Butsugan, Y. *J. Mater. Sci.* **1995**, *30*, 837.